electronics

MDPI

Article

Memory Characteristics of Thin Film Transistor with Catalytic Metal Layer Induced Crystallized Indium-Gallium-Zinc-Oxide (IGZO) Channel

Hoonhee Han, Seokmin Jang, Duho Kim, Taeheun Kim, Hyeoncheol Cho, Heedam Shin and Changhwan Choi *

Division of Material Science and Engineering, Hanyang University, Seoul 04763, Korea; gksgnsgnl@hanyang.ac.kr (H.H.); univash94@hanyang.ac.kr (S.J.); duho96@hanyang.ac.kr (D.K.); kth6604@hanyang.ac.kr (T.K.); xienz7766@hanyang.ac.kr (H.C.); heedarm@hanyang.ac.kr (H.S.)
* Correspondence: cchoi@hanyang.ac.kr

Abstract: The memory characteristics of a flash memory device using c-axis aligned crystal indium gallium zinc oxide (CAAC-IGZO) thin film as a channel material were demonstrated. The CAAC-IGZO thin films can replace the current poly-silicon channel, which has reduced mobility because of grain-induced degradation. The CAAC-IGZO thin films were achieved using a tantalum catalyst layer with annealing. A thin film transistor (TFT) with $SiO_2/Si_3N_4/Al_2O_3$ and CAAC-IGZO thin films, where Al_2O_3 was used for the tunneling layer, was evaluated for a flash memory application and compared with a device using an amorphous IGZO (*a*-IGZO) channel. A source and drain using indium-tin oxide and aluminum were also evaluated for TFT flash memory devices with crystallized and amorphous channel materials. Compared with the *a*-IGZO device, higher on-current (I_{on}), improved field effect carrier mobility (μ_{FE}), a lower body trap (N_{ss}), a wider memory window (ΔV_{th}), and better retention and endurance characteristics were attained using the CAAC-IGZO device.

Keywords: CAAC-IGZO; NAND flash; thin film transistor; high-k

Citation: Han, H.; Jang, S.; Kim, D.; Kim, T.; Cho, H.; Shin, H.; Choi, C. Memory Characteristics of Thin Film Transistor with Catalytic Metal Layer Induced Crystallized Indium-Gallium-Zinc-Oxide (IGZO) Channel. *Electronics* **2022**, *11*, 53. https://doi.org/10.3390/electronics11010053

Academic Editor: Antonio Di Bartolomeo

Received: 12 November 2021
Accepted: 15 December 2021
Published: 24 December 2021

1. Introduction

Flash memory devices have evolved from two-dimensional to three-dimensional (3D) structures, which enable better performance and higher density, enabling large capacity data storage [1–3]. Polycrystalline silicon (poly-Si) is a necessary component to form 3D NAND flash memory as a channel material. However, there are several issues in using poly-Si for 3D flash devices [4]. For example, the poly-Si channel material causes mobility degradation, high current leakage, and threshold voltage (V_{th}) variation because poly grains induce degradation, including scattering at grain boundaries and random distribution of the grain shape and size. Additionally, poly-Si suffers from temperature instability. Therefore, there is a growing need for alternative channel materials such as indium-gallium-zinc oxide (IGZO). Since IGZO was discovered in 2004, thin film transistor (TFT) devices using amorphous IGZO (*a*-IGZO) semiconductor material have received attention as the back plane of flat panel display applications because of their high field effect mobility [4–21]. In this regard, *a*-IGZO was demonstrated as a channel material in a flash memory device. However, because of the nature of the amorphous material, *a*-IGZO also has limited mobility, V_{th} variation, and weak resistance to electrical stress [22]. Therefore, new oxide semiconductor materials are required. Compared with the amorphous structure, a crystalline structure has a low density of defect states, thereby suppressing carrier scattering and leading to improved device performance. A new crystalline structure, c-axis-aligned crystalline (CAAC) IGZO thin film material, is of great interest because of its improved mobility and stability [23–34]. A CAAC-IGZO-based field effect transistor (FET) device achieved very low off-leakage current (I_{off}) down to yocto ampere (10^{-24} A/μm) because of the wider bandgap than that of conventional Si-based FET and effective suppression of the short-channel effects [24,25]. A CAAC-IGZO structure can be formed through

various methods, such as Ta metal-induced crystallization [22] and substrate heating during sputter deposition [28,29], and the structure has been applied to memory and sensor devices [35–37]. However, studies applying these CAAC-IGZO materials to flash memory devices are limited. $SiO_2/Si_3N_4/SiO_2$ (ONO) layers can also be replaced by high-*k* thin film to enhance the flash memory performance [38–41]. Therefore, research on flash memory devices using CAAC-IGZO channel materials and high-*k* thin film is of great interest.

Our work focuses on the effect of crystallized IGZO material as a channel for the flash memory device application as an alternative to current poly-Si and *a*-IGZO materials. Even though many amorphous oxide semiconductor materials have been explored as the channel material within the flash memory, crystallized oxide semiconductors have not been investigated yet with a high-*k* layer as a tunneling layer (TNL) and alternative source and drain (S/D) material to further improve flash memory characteristics. The crystallized oxide semiconductor is superior to the amorphous oxide semiconductor in terms of transistor characteristics and memory behavior.

In this study, CAAC-IGZO thin film was realized by a heat-treated catalytic transition metal layer on an *a*-IGZO thin film, and the film was applied as a channel material to a TFT-type flash memory device. In addition, Al_2O_3, a high-*k* thin film, was used as the TNL, and different materials were studied for the S/D. To evaluate the performance improvement of the flash memory, TFT flash devices based on the *a*-IGZO channel were compared. The TFT flash memory device using CAAC-IGZO exhibits low leakage current and high mobility, and the additional use of high-*k* TNL and aluminum (Al) S/D contact provides a wider memory window.

2. Experiment

Before TFT-type flash memory fabrication, the conversion from *a*-IGZO to a CAAC-IGZO layer was achieved by the catalytic transition metal layer via post annealing and its crystallinity was confirmed. First, a 15-nm thick *a*-IGZO film was deposited on a Si substrate or insulating film. This IGZO was deposited with a shadow mask (width/length = 700 μm/700 μm) by RF sputtering at 100 watts, a working pressure of 4 mTorr, and ambient Ar. This IGZO serves as the active layer for the back gate TFT. To form the CAAC-IGZO thin film, a 20 nm thick Ta thin film was deposited on *a*-IGZO, and then heat treated in an O_2 atmosphere at a low temperature of 300 °C for 1 h.

This catalyst layer was formed in the 150 μm dimension located in the middle of *a*-IGZO thin film [22]. During this heat treatment process, Ta acts as a catalyst to convert the amorphous phase into a crystalline thin film. X-ray diffraction (XRD) and high-resolution transmission (HRTEM) were used to confirm the crystallinity of IGZO layers.

A flash memory device using a CAAC-IGZO layer with a thickness of 10 to 30 nm was fabricated and evaluated as a channel material, and the IGZO thin film was crystallized by the metal catalyst method described above. The flash memory device was fabricated with a TFT structure having a back gate. First, SiO_2 and Si_3N_4 thin films were formed by PECVD as the blocking oxide (BKL) and charge trap layer (CTL), respectively, on a heavily doped p-type Si wafer substrate as a bottom gate electrode. The TNL was SiO_2 or Al_2O_3. $SiO_2/Si_3N_4/Al_2O_3$ is denoted as ONA. To study the memory window, BKL/CTL/TNL was changed to a thickness of 5/7/5 nm or 20/15/6 nm. S/D layers were formed by sputtering indium-tin oxide (ITO) or Al, and patterns were formed using a shadow mask or photolithography. These devices were processed by post-deposition annealing in an O_2 atmosphere at 300 °C for 1 h. To compare the effect on the crystallinity of the IGZO thin film, an *a*-IGZO thin film device was also fabricated and compared. The cross-sectional data of the CAAC-IGZO-based flash device was obtained through atomic composition data of the TEM analysis and EDS analysis, and the memory window, which is a characteristic of flash memory, was evaluated by applying a programing and erasing voltage (V_{PROG} and V_{ERASE}) pulse of 18 to 20 V at the gate for 1 ms.

3. Results and Discussion

Figure 1 compares the XRD spectra for IGZO crystallization between *a*-IGZO and CAAC-IGZO. The Ta-capped IGZO film has two distinct peaks, and a crystallized IGZO (009) XRD peak was detected near 32°; however, no peak was observed in the case of *a*-IGZO. The XRD peak near 38.5° corresponds to the tetragonal b-Ta metal layer (110) [42].

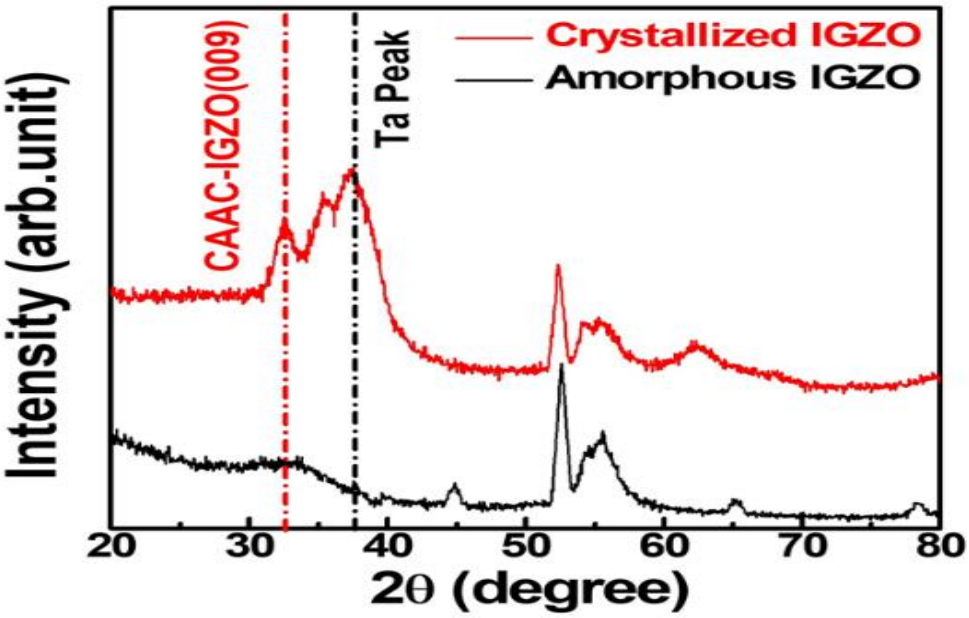

Figure 1. XRD spectra of the IGZO thin film without and with Ta metal film that was annealed at 300 °C under O_2 ambient for 1 h.

Figure 2 shows the surface roughness images of IGZO on the SiO_2 or Al_2O_3 layers using an atomic force microscope (AFM). In the TFT flash memory device structure, because the active IGZO layer was formed on TNL, SiO_2, and Al_2O_3, it was necessary to check the surface roughness. The surface roughness of the SiO_2 layer was smoother than that of Al_2O_3 before *a*-IGZO deposition [43,44]. However, when *a*-IGZO was deposited, the surface roughness of SiO_2 and Al_2O_3 increased from 0.345 to 2.78 nm and from 0.697 to 1.20 nm, respectively; however, Al_2O_3 was less rough than *a*-IGZO/SiO_2. As previously reported, the Al_2O_3 film containing crystalline material is stable in *a*-IGZO because of the low defect concentration; however, the SiO_2 film containing amorphous material has more defects [43].

Figure 3a,b show the TEM and structural images of flash memory devices with *a*-IGZO and CAAC-IGZO channel materials, respectively. Compared with the *a*-IGZO layer, the crystalline domains appear clearly within the CAAC-IGZO layer with the Ta catalyst layer, indicating that Ta atoms can induce atomic rearrangement in the *a*-IGZO layer and convert to the CAAC-IGZO layer. The EDS profile shows the atomic content through the structure, where the Ta atoms remain in their original state without penetration. In addition, the oxygen distributed in the crystallization process by the Ta metal layer in the IGZO layer was confirmed. Therefore, a good interface with stable crystalline IGZO was obtained, and it was expected that high-performance TFTs could be formed and good flash memory behavior achieved.

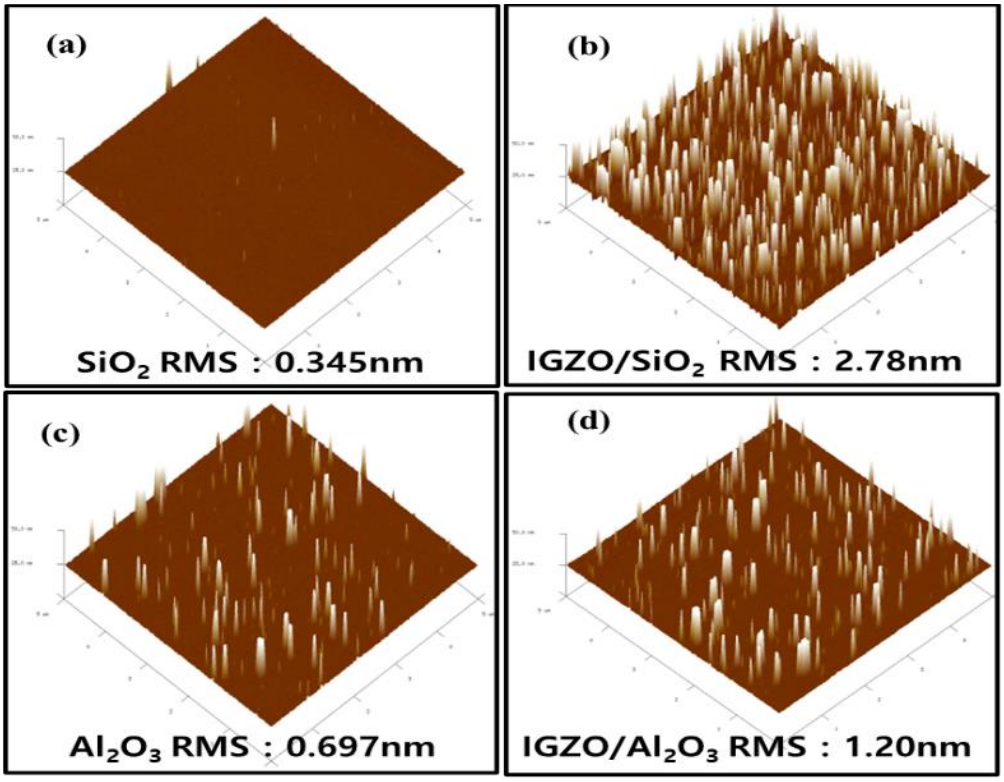

Figure 2. AFM images of (**a**) SiO_2, (**b**) IGZO on SiO_2, (**c**) Al_2O_3, and (**d**) IGZO on Al_2O_3 where SiO_2 and Al_2O_3 serve as the TNL in the TFT flash memory device.

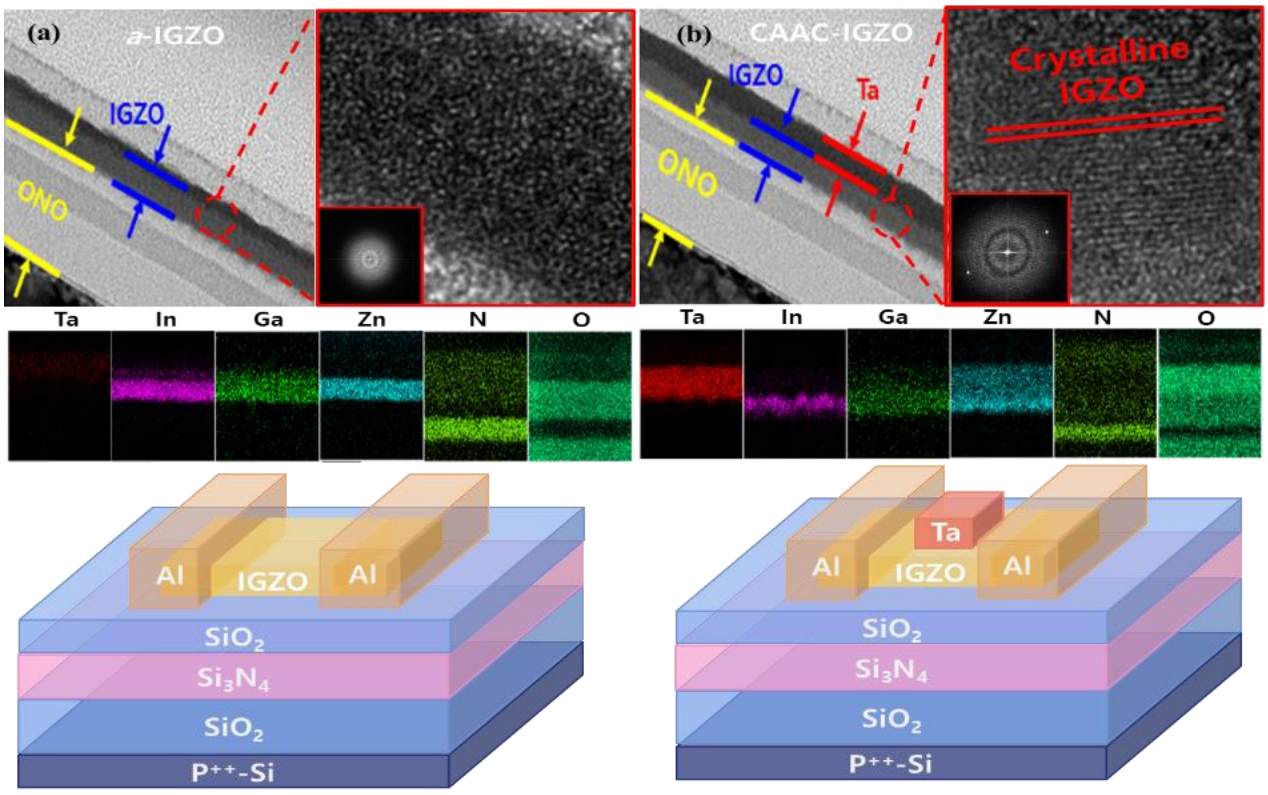

Figure 3. Cross-sectional flash memory TEM images and device schemes with (**a**) *a*-IGZO and (**b**) CAAC-IGZO layers.

Figure 4 compares the characteristics of the *a*-IGZO TFT flash memory devices with ONO and ONA. The energy band diagrams of each case are shown in Figure 4a. A memory window via a change in threshold voltage (ΔV_{th}) was obtained by adjusting a program voltage of 20 V and a program pulse time (1 ms to 100 ns) in a back gate transistor-based flash device (ONO and ONA: 20/15/6 nm). A more effective V_{th} change was obtained when Al_2O_3 was used as a TNL with a low bandgap compared with that of SiO_2, as shown in Figure 4b,c. This superiority of Al_2O_3 to SiO_2 was confirmed at the interface and in the operating performance of the flash device [45] because Al_2O_3 has greater electron affinity and a lower band gap [42], which contributes to easy passage of the carriers through the barrier.

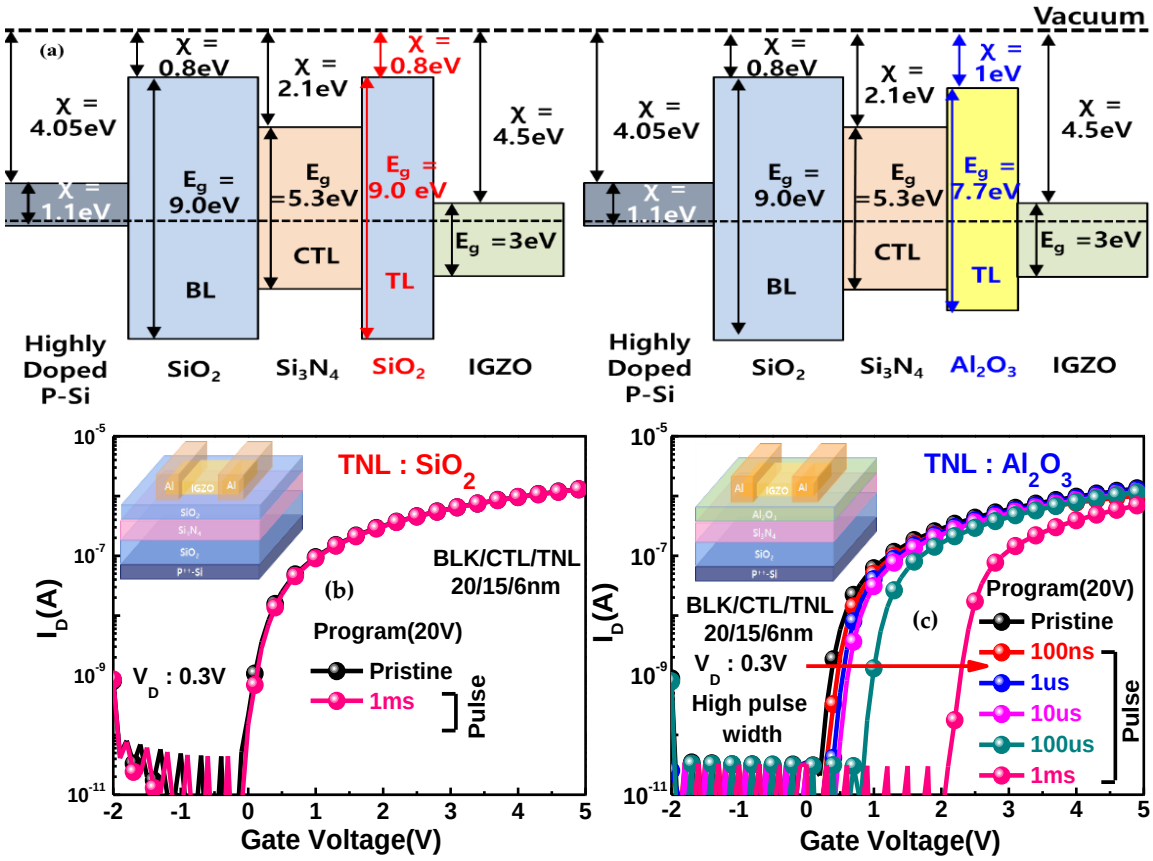

Figure 4. Schematics of (**a**) the energy band diagrams of TFT flash memory devices with SiO_2 and Al_2O_3 as the TNL. Programing behaviors under various pulse times for *a*-IGZO TFT flash memory devices with (**b**) SiO_2 and (**c**) Al_2O_3 TNLs.

For the performance evaluation of the *a*-IGZO and CAAC-IGZO devices, the transfer characteristic (I_d-V_g) was compared, as shown in Figure 5. Different thicknesses (10 and 30 nm) of the active channel layer and tunneling oxide type (SiO_2 and Al_2O_3) were used. Compared with the *a*-IGZO device shown in Figure 5a, the CAAC-IGZO device exhibited improved mobility, lower interface state density (D_{it}), and better V_{th} stability with the active layer thickness (Figure 5b). These characteristics were attributed to less oxygen vacancy in the crystallized IGZO than in *a*-IGZO [22,46–50]. These results indicate that the crystallinity of the channel material is an important parameter to enhance device performance. In addition, the device performance is also affected by the active layer thickness and tunneling oxide. Figure 5c compares the mobility and D_{it} for both devices. For the *a*-IGZO device, an the field effect mobility (μ_{FE}) was approximately 17 cm^2/Vs for the IGZO thickness range from 10 to 30 nm. Alternatively, the CAAC-IGZO device has an μ_{FE} of approximately 43 cm^2/Vs for the same thickness range. The crystallized channel could effectively suppress the subthreshold swing (SS) degradation. The D_{it} of

the *a*-IGZO device was 2.5 × 10^{12} $cm^{-2}ev^{-1}$, whereas that of the CAAC-IGZO device was 1.2 × 10^{12} $cm^{-2}ev^{-1}$, where D_{it} was extracted from the SS value [51]. This improvement of the proposed CAAC-IGZO device structure was similar to other reported crystalline IGZO channel-based devices [42]. Figure 5d compares the device parameters of the mobility and SS in our devices with previously reported devices. The crystallized IGZO shows an improvement over *a*-IGZO and our materials show better enhancement than the other crystallized IGZO materials. The crystallization is also helpful to improve the interface quality.

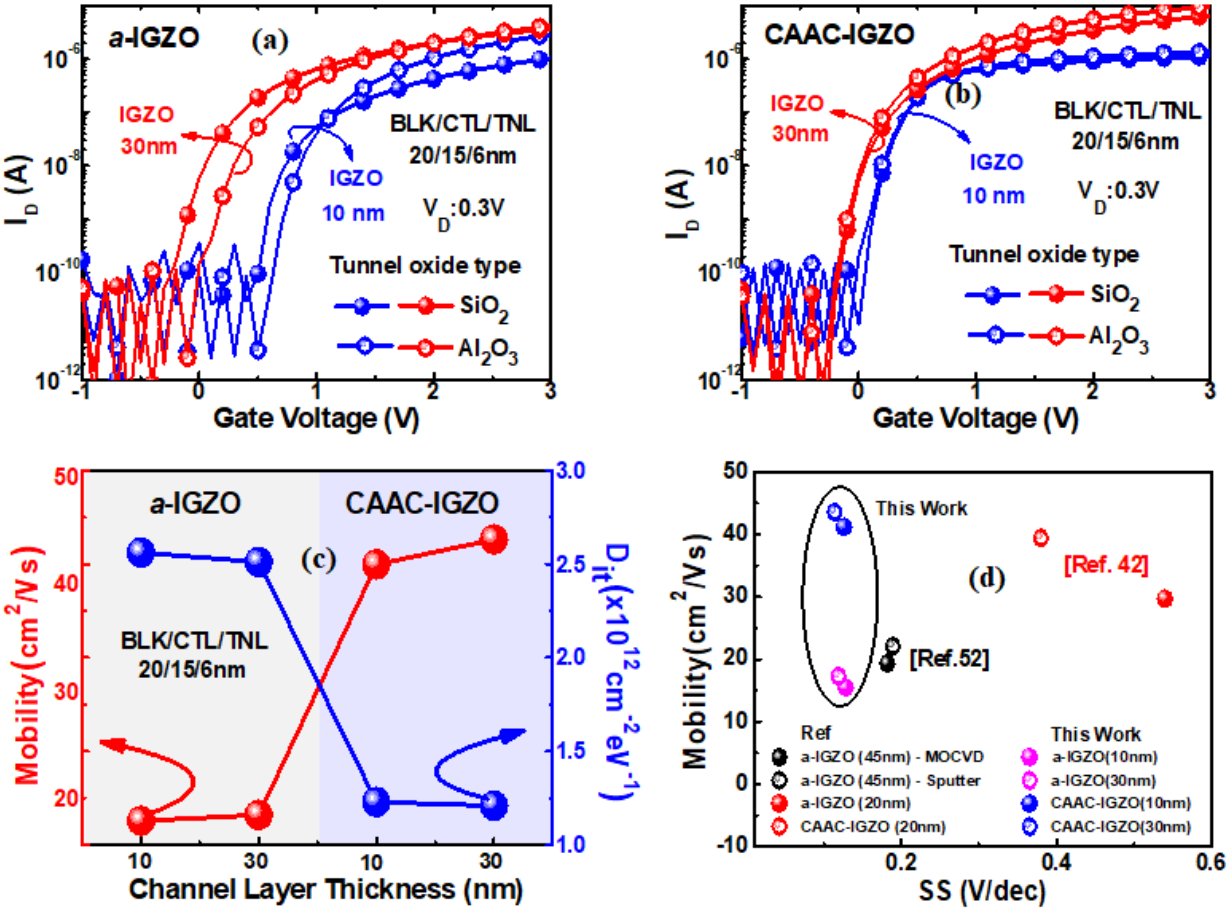

Figure 5. I_d–V_g comparison of the (**a**) *a*-IGZO and (**b**) CAAC-IGZO devices. (**c**) Dependence of the active layer thickness on μ_{FE} and D_{it}. (**d**) Comparison of reported IGZO-based devices with this work [42,52].

For program characteristic between two devices, various measurement conditions were applied, as shown in Figure 6. These devices have SiO_2 and Al_2O_3 as a TNL, and the film thickness was reduced from 20/15/6 nm to 5/7/5 nm for BKL/CTL/TNL. Using ONO thin films, compared with the *a*-IGZO device, a slightly wider V_{th} shift was attained using the CAAC-IGZO device even for different measurement pulse widths, as shown in Figure 6a,b. The V_{th} shift values were 0.66 and 0.74 V under a 100 µs pulse width for amorphous and crystallized devices, respectively, and the difference increased as the pulse width was reduced. Using Al_2O_3 as a TNL, better programming behavior was achieved. Compared to the device using SiO_2 as a TNL, when Al_2O_3 was used as TNL, the *a*-IGZO device improved the programming characteristics by 28~35% and CAAC-IGZO device by 30–36%, and the crystallized channel device was still superior to the amorphous channel device. This advantage occurs because the fast carrier mobility can easily trap electrons in the CTL [42]. Figure 6c compares the programming characteristic with channel materials and TNL type with respect to the pulse width from 10^{-6} to 10^{-3} s at a 20 V programing

voltage. The active layer crystallization and adoption of Al_2O_3 as a TNL clearly improved the programing characteristics.

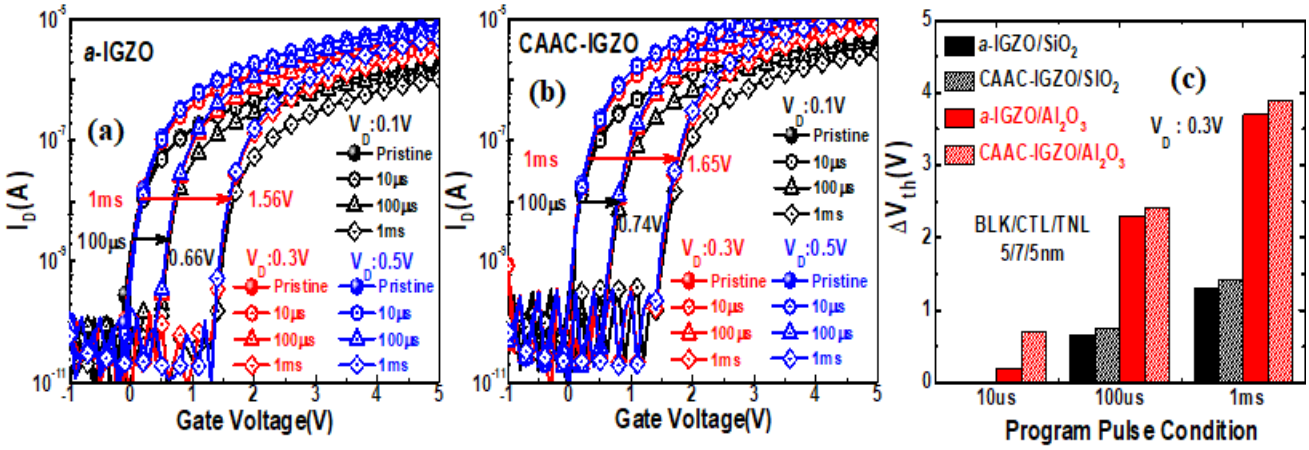

Figure 6. Memory performance of devices using amorphous and crystallized IGZO active layers with different pulse conditions: (**a**) a-IGZO and (**b**) CAAC-IGZO. (**c**) V_{th} shift for different TNLs and program pulses.

ITO and Al were used for S/D regions to improve the memory window of the IGZO-based flash memory device. Using capacitor devices, we demonstrated that the flash operation depends on the S/D contact metals, as shown in Figure 7. Compared with ITO metal, the flat band voltage shift (C–V shift) was enhanced using the Al metal contact in the capacitor device, as shown in Figure 7b,d. This wider memory window was attributed to different band gap properties of the metal and IGZO layers. Figure 7a,c shows the corresponding energy band diagram of the corresponding capacitors with different metal contacts and IGZO active material. The barrier of the IGZO/metal (ITO [53] and Al [54]) can block the electron sinking from IGZO to the metal under pulse conditions; as a result, the Al metal contact can easily make electrons sink because of its lower electron affinity than that of IGZO [42]. Thus, the S/D contact metal is also an important parameter to increase the performance of IGZO-based flash memory with an Al_2O_3 TNL and the crystallized active channel material.

Based on the findings of the effect of S/D metal contact, the memory window was also studied in a back gate TFT. Figure 8 shows transfer characteristics of amorphous and crystallized IGZO-based flash memory with a S/D contact of ITO and Al metal. Figure 8a,c show *a*-IGZO devices with ITO and Al, respectively, while Figure 8b,d how CAAC-IGZO devices with ITO and Al, respectively. The TNL is Al2O3 and the active layer thickness is 15 nm. The flash memory operation properties with *a*-IGZO and CAAC-IGZO active layers were attained by applying a $V_{PROG/ERASE}$ pulse of ±18 V range for 1 ms for V_D = 0.3 V. For both devices with Al for a S/D contact, a V_{th} shift was observed; however, a larger window occurred for the CAAC-IGZO device. The V_{th} shift of the amorphous and crystallized active channel devices were 0.28 and 0.4 V, respectively. However, the *a*-IGZO and CAAC-IGZO devices with ITO for a S/D contact had a negligible or narrower memory window than the Al for a S/D contact metal even though a higher $V_{PROG/ERASE}$ pulse of ±20 V for 1 ms was applied, as shown Figure 8a,b. This result suggests that the S/D contact metal significantly influences the flash memory operation.

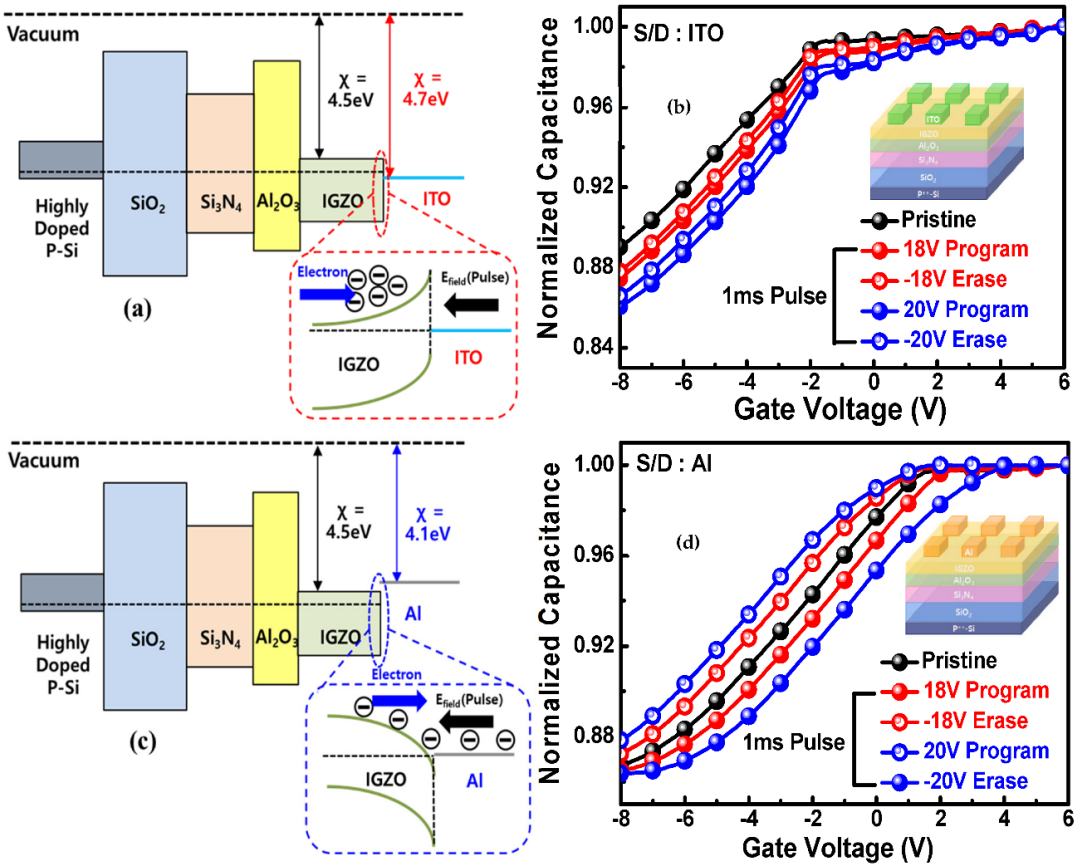

Figure 7. Schematics of energy diagrams: (**a**) a-IGZO/ITO and (**c**) a-IGZO/Al, C-V characteristic (**b**) a-IGZO/ITO and (**d**) a-IGZO/Al.

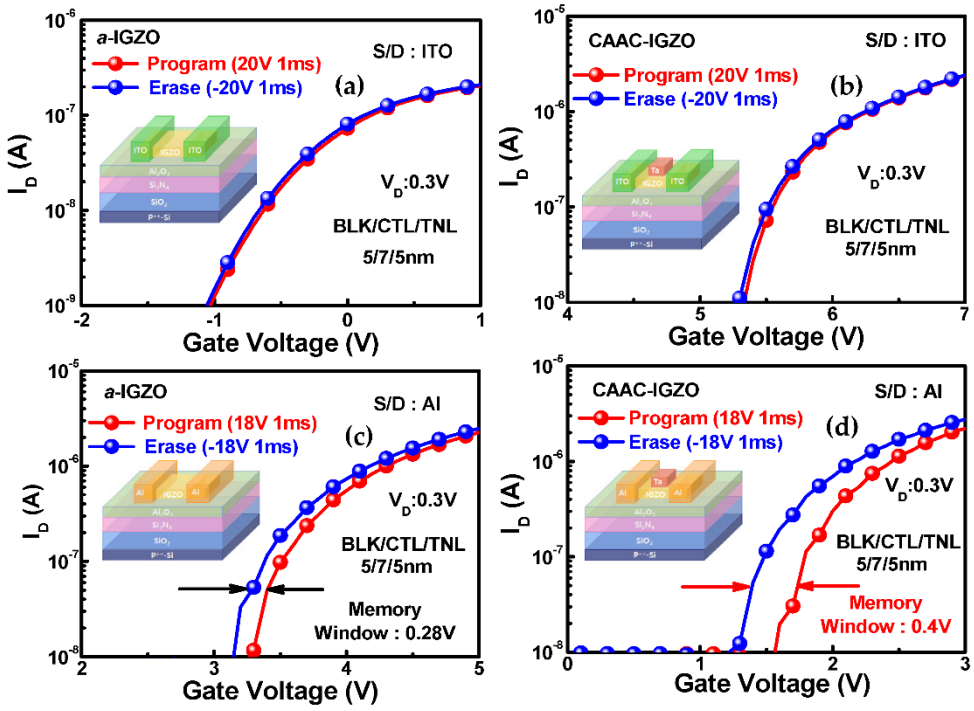

Figure 8. Transfer characteristics of the *a*-IGZO and CAAC-IGZO devices with different S/D materials: (**a**,**c**) show *a*-IGZO devices with ITO and Al for S/D, respectively, and (**b**,**d**) show CAAC-IGZO devices with ITO and Al for S/D, respectively.

Reliability characteristics, such as endurance and retention, were investigated to determine if the crystallized IGZO active channel material maintains its superiority over amorphous IGZO material. Figure 9 shows the retention characteristics for amorphous and crystallized IGZO channel devices using Al_2O_3 as TNL. Figure 9a,b corresponds to the retention behaviors of the *a*-IGZO and CAAC-IGZO channel devices, respectively, where the charge loss state was tested for up to 10^4 s. The memory window of the CAAC-IGZO device was wider and more stable than that of the *a*-IGZO device, indicating that the CAAC-IGZO active channel was quite stable. The charge of the *a*-IGZO-based flash memory can easily be lost at low bias. The *a*-IGZO and CAAC-IGZO-based devices were expected to have charge loss degradation of 39% and 65%, respectively, over 10 years from their pristine state. As previously reported, the crystallized IGZO-based flash memory retention can suppress the charge loss more than the amorphous IGZO channel device [42].

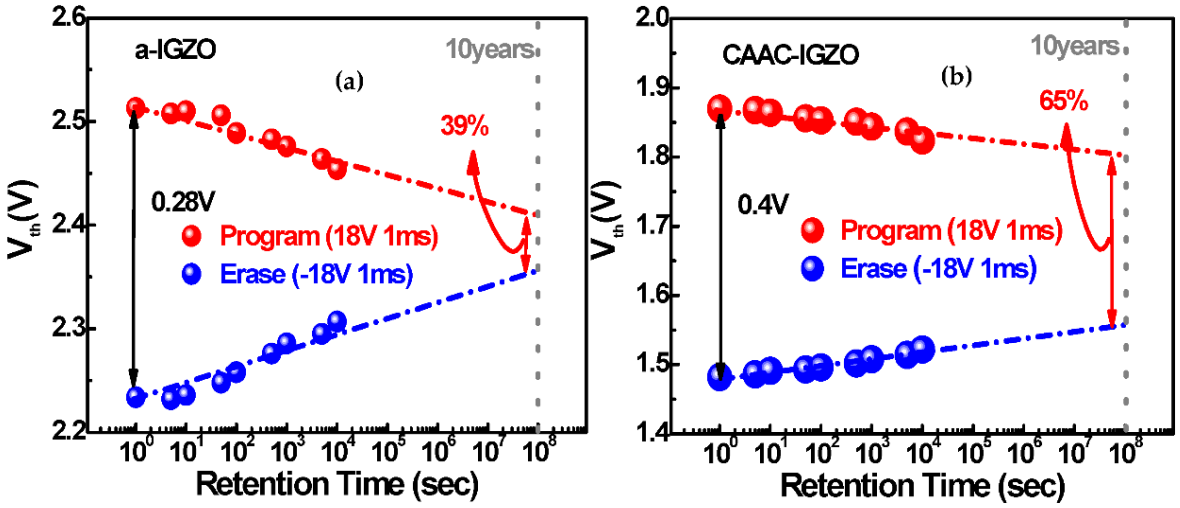

Figure 9. Retention characteristics of (**a**) *a*-IGZO and (**b**) CAAC-IGZO devices tested up to 10^4 s.

The endurance characteristics of the amorphous and crystallized IGZO channel devices up to 10^4 cycles are shown in Figure 10a,b, respectively. Both devices increased in terms of V_{th} shift during the program and erase pulse cycling. However, the endurance degradation of the crystallized IGZO device was less than that of the amorphous IGZO device. Similar to the retention behavior, the crystallized active layer provides more suitable memory properties than the amorphous layer.

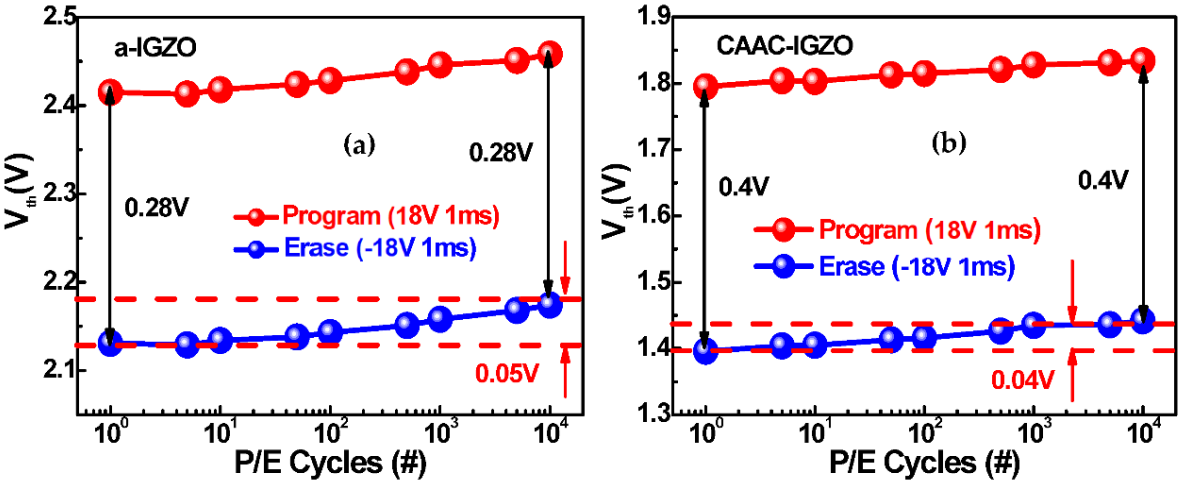

Figure 10. Endurance characteristics of (**a**) *a*-IGZO and (**b**) CAAC-IGZO devices tested up 10^4 cycles.

4. Conclusions

In summary, we demonstrated a metal-induced c-axis crystallized IGZO-based flash memory with excellent performance compared with an *a*-IGZO device. The CAAC-IGZO layer shows improved μ_{FE}, SS, and I_{on}. In conjunction with Al_2O_3 as the TNL and Al as the S/D metal, the CAAC-IGZO flash memory exhibits a wider memory window and superior endurance and retention characteristics, indicating that crystallized IGZO may be an alternative channel material for advanced flash memory device applications.

Author Contributions: Methodology, paper writing, investigation, conceptualization, H.H.; Validation, S.J., D.K., T.K., H.C., H.S.; funding acquisition, supervision and editing, C.C. All authors have read and agreed to the published version of the manuscript.

Funding: This work supported by the Future Semiconductor Device Technology Development Program (10080689, 20003808, 20004399) funded by MOTIE (Ministry of Trade, Industry & Energy) and KSRC (Korea Semiconductor Research Consortium), This research was supported by the BK21 FOUR (Fostering Outstanding Universities for Research) project of the National Research Foundation of Korea Grant.

Conflicts of Interest: The authors declare no conflict of interest.

References

1. Lue, H.T.; Lai, S.C.; Hsu, T.H.; Hsiao, Y.H.; Du, P.Y.; Wang, S.Y.; Hsieh, K.Y.; Liu, R.; Lu, C.Y. A critical review of charge-trapping NAND flash devices. In Proceedings of the 2008 9th International Conference on Solid-State and Integrated-Circuit Technology, Beijing, China, 20–23 October 2008; p. 4734663.
2. Zhao, C.; Zhao, C.Z.; Taylor, S.; Chalker, P.R. Review on non-volatile memory with high-k dielectric: Flash for generation beyond 32 nm. *Materials* **2014**, *7*, 5117–5145. [CrossRef]
3. Ramkumar, K.; Prabhakar, V.; Keshavarzi, A.; Kouznetsov, I.; Geha, S. SONOS memories: Advances in materials and devices. *MRS Adv.* **2017**, *2*, 209–221. [CrossRef]
4. Compagnoni, C.M.; Goda, A.; Spinelli, A.S.; Feeley, P.; Lacaita, A.L.; Visconti, A. Reviewing the evolution of the NAND flash technology. *Proc. IEEE* **2017**, *105*, 1609. [CrossRef]
5. Nomura, K.; Ohta, H.; Takagi, A.; Kamiya, T.; Hirano, M.; Hosono, H. Room-temperature fabrication of transparent flexible thin-film transistors using amorphous oxide semiconductors. *Nature* **2004**, *432*, 488–492. [CrossRef]
6. Jianhen, S.; Hong, T.; Lee, H.-M.; Kim, K.; Sasase, M.; Kim, J.; Hosono, H.; Park, J.-S. Amorphous IGZO TFT with High Mobility of ~70 cm^2/(Vs) via Vertical Dimension. *ACS Appl. Mater. Interfaces* **2004**, *11*, 40300–40309.
7. Oota, M.; Ando, Y.; Tsuda, K.; Koshida, T.; Oshita, S.; Suzuki, A.; Fukushima, K.; Nagatsuka, S.; Onuki, T.; Hodo, R.; et al. 3D-stacked CAAC-In-Ga-Zn Oxide Fets with Gate Length of 72 nm. In Proceedings of the 2019 IEEE International Electron Devices Meeting (IEDM), San Francisco, CA, USA, 7–11 December 2019.
8. Wu, K.; Zhang, J.; Li, Y.; Wang, X.; Liu, Y.; Yu, Q.; Chen, T. Design of AM Self-Capacitive Transparent Touch Panel Based on a-IGZO Thin-Film Transistors. *IEEE Access* **2020**, *2989435*, 76929–76934. [CrossRef]
9. Cho, M.H.; Choi, C.H.; Seul, H.J.; Cho, H.C.; Jeong, J.K. Achieving a Low-Voltage, High-Mobility IGZO Transistor through and ALD-Derived Bilayer Channel and a Hafnia-Based Gate Dielectric Stack. *ACS Appl. Mater. Interfaces* **2021**, *13*, 16628–16640. [CrossRef] [PubMed]
10. Samanta, S.; Chand, U.; Xu, S.; Han, K.; Wu, Y.; Wang, C.; Kumar, A.; Velluri, H.; Li, Y.; Fong, X.; et al. Low Subthreshold Swing and High Mobility Amorphous Indium-Gallium-Zinc-Oxide Thin-Film Transistor with Thin HfO_2 Gate Dielectric and Excellent Uniformity. *IEEE Electron Device Lett.* **2020**, *41*, 856–859. [CrossRef]
11. Chu, Y.L.; Young, S.-J.; Ji, L.-W.; Yan, S.-P. Fabrication and Characterization of a-IGZO Thin-Film Transistors with and without Passivation Layers. *ECS J. Solid State SCI. Technol.* **2021**, *10*, 027002. [CrossRef]
12. Jeon, S.; Ahn, S.-E.; Song, I.; Kim, C.J.; Chung, U.-I.; Lee, E.; Yoo, I.; Nathan, A.; Lee, S.; Ghaffarzadeh, K.; et al. Gated three-terminal device architecture to eliminate persistent photoconductivity in oxide semiconductor photosensor arrays. *Nat. Mater.* **2012**, *11*, 301–305. [CrossRef] [PubMed]
13. Yu, Y.; Lv, N.; Zhang, D.; Wei, Y.; Wang, M. High-Mobility Amorphous InGaZnO Thin-Film Transistors with Nitrogen Introduced Via Low-Temperature Annealing. *IEEE Electron Device Lett.* **2021**, *42*, 1480–1483. [CrossRef]
14. Koretomo, D.; Shuhei, H.; Marin, M.; Yusaku, M.; Mamoru, F. Marked improvement in reliability of 150 °C processed IGZO thin-film transistors by applying hydrogenated IGZO as a channel material. *Appl. Phys. Express* **2020**, *13*, 076501. [CrossRef]
15. Cho, M.H.; Seol, H.; Song, A.; Choi, S.; Song, Y.; Yun, P.S.; Chung, K.-B.; Bae, J.U.; Park, K.-S.; Jeong, J.K. Comparative Study on Performance of IGZO Transistors With Sputtered and Atomic Layer Deposited Channel Layer. *IEEE Trans. Electron Devices* **2019**, *66*, 1780–1788. [CrossRef]
16. Mo, F.; Tagawa, Y.; Jin, C.; Ahn, M.; Saraya, T.; Hiramoto, T.; Kobayashi, M. Low-Voltage Operating Ferroelectric FET with Ultrathin IGZO Channel for High-Density Memory Application. *IEEE J. Electron Devices Soc.* **2020**, *8*, 717–723. [CrossRef]

17. Shi, L.; Wang, J.; Zhang, Y. Synergistic improvement of device performance and bias stress stability of IGZO TFT via back-channel graded nitrogen doping. *Mater. Lett.* **2021**, *305*, 130749. [CrossRef]
18. Kim, Y.S.; Lee, M.-H.; Lim, J.H.; Park, J.-S. Impact of tandem IGZO/ZnON TFT with energy-band aligned structure. *Appl. Phys. Lett.* **2020**, *117*, 143505. [CrossRef]
19. Park, C.B.; Na, H.I.; Yoo, S.S.; Park, K.-S. Electromechanical properties of amorphous indium-gallium-zinc-oxide transistors structured with an island configuration on plastic. *Appl. Phys. Express* **2016**, *9*, 031101. [CrossRef]
20. Kim, W.-G.; Tak, Y.J.; Ahn, B.D.; Jung, T.S.; Chung, K.-B.; Kim, H.J. High-pressure gas activation for amorphous indium-gallium-zinc-oxide thin-film transistors at 100 °C. *Sci. Rep.* **2016**, *6*, 23039. [CrossRef] [PubMed]
21. Petti, L.; Munzenrieder, N.; Vogt, C.; Faber, H.; Buthe, L.; Cantarella, G.; Bottacchi, F.; Anthopoulos, T.D.; Troster, G. Metal oxide semiconductor thin-film transistor for flexible electronics. *Appl. Phys. Rev.* **2016**, *3*, 021303. [CrossRef]
22. Shin, Y.; Kim, S.T.; Kim, K.; Kim, M.Y.; Oh, S.; Jeong, J.K. The mobility enhancement of indium gallium zinc oxide transistors via low-temperature crystallization using a tantalum catalytic layer. *Sci. Rep.* **2017**, *7*, 10885. [CrossRef] [PubMed]
23. Suzuki, A.; Yuichi, Y.; Mizukami, S.; Tsuda, K.; Ito, M.; Ohchima, K.; Matsumoto, N.; Yakubo, Y.; Miyata, S.; Okuno, N.; et al. Characteristics and Application of CAAC-IGZO FET with Gate Length of 13 nm. *ECS Trans.* **2020**, *98*, 13–27. [CrossRef]
24. Kato, K.; Shionoiri, Y.; Sekine, Y.; Furutani, K.; Hatano, T.; Aoki, T.; Sasaki, M.; Tomatsu, H.; Koyama, J.; Yamazaki, S. Evaluation of off-state current characteristics of transistor using oxide semiconductor material, indium-gallium-zinc oxide. *Jpn. J. Appl. Phys.* **2012**, *5*, 021201. [CrossRef]
25. Kobayashi, Y.; Matsudo, S.; Matsubayashi, D.; Suzawa, H.; Sakakura, M.; Hanaoka, K.; Okazaki, Y.; Yamamoto, T.; Hondo, S.; Hamada, T.; et al. Electrical characteristics and short-channel effect of c-axis aligned crystal indium gallium zinc oxide transistor with short channel length. *Jpn. J. Appl. Phys.* **2014**, *53*, 04EF03. [CrossRef]
26. Kang, Y.; Lee, W.; Kim, J.; Keum, K.; Kang, S.-H.; Jo, J.-W.; Park, S.K.; Kim, Y.-H. Effects of crystalline structure of IGZO thin films on the electrical and photo-stability of metal-oxide thin-film transistors. *Mater. Res. Bull.* **2021**, *139*, 111252. [CrossRef]
27. Kurokawa, Y.; Aoki, T.; Kozuma, M.; Kimura, H.; Kanemura, T.; Ando, Y.; Yamazaki, S. CAAC-IGZO FET/Si-FET hybrid structured analog multiplier and vector-by-matrix multiplier for neural network. *Jpn. J. Appl. Phys.* **2020**, *59*, SGGB03. [CrossRef]
28. Yamazaki, S.; Atsumi, T.; Dairiki, K.; Okazaki, K.; Kimizuka, N. In-Ga-Zn-Oxide semiconductor and its transistor characteristics. *ECS J. Solid State Sci. Technol.* **2014**, *3*, Q3012–Q3022. [CrossRef]
29. Yamazaki, S.; Yamazaki, S.; Suzawa, H.; Inoue, K.; Kato, K.; Hirohashi, T.; Okazaki, K.; Kimizuka, N. Properties of crystalline In-Ga-Zn-oxide semiconductor and its transistor characteristics. *Jpn. J. Appl. Phys.* **2014**, *53*, 04ED18. [CrossRef]
30. Wang, X.; Shen, Z.; Li, J.; Wu, S. Preparation and Properties of Crystalline IGZO Thin Films. *Membrane* **2021**, *11*, 134. [CrossRef] [PubMed]
31. Kunitake, H.; Ohshima, K.; Tsuda, K.; Matsumoto, N.; Koshida, T.; Ohshita, S.; Sawai, H.; Yanagisawa, Y.; Saga, S.; Arasawa, R.; et al. A C-Axis-Aligned Crystalline In-Ga-Zn Oxide FET with a Gate Length of 21 nm Suitable for Memory Applications. *IEEE J. Electron Devices Soc.* **2019**, *7*, 495–502. [CrossRef]
32. Setten, M.J.V.; Dekkers, H.F.W.; Kljucar, L.; Mitard, J.; Pashartis, C.; Subhechha, S.; Rassoul, N.; Delhougne, R.; Kar, G.S.; Pourtois, G. Oxygen Defect Stability in Amorphous, C-Axis Aligned, and spinel IGZO. *ACS Appl. Electron. Mater.* **2021**, *3*, 4037–4046. [CrossRef]
33. Hwang, A.Y.; Kim, S.T.; Ji, H.; Shin, Y.; Jeong, J.K. Metal-induced crystallization of amorphous zinc tin oxide semiconductors for high mobility thin-film transistors. *Appl. Phys. Lett.* **2016**, *108*, 152111. [CrossRef]
34. Zhang, J.; Wen, X.; Hu, L.; Xu, W.; Zhu, D.; Cao, P.; Liu, W.; Han, S.; Liu, X.; Jia, F.; et al. C-axis oriented crystalline IGZO thin-film transistors by magnetron sputtering. *J. Mater. Chem. C* **2017**, *5*, 2388. [CrossRef]
35. Kurokawa, Y.; Okamoto, Y.; Nakagawa, T.; Aoki, T.; Ikeda, M.; Kozuma, M.; Osada, T.; Ikeda, T.; Yamade, N.; Okazaki, Y.; et al. Applications of crystalline indium-gallium-zinc-oxide technology to LSI: Memory, processor, Image sensor, and field programmable gate array. In Proceedings of the Fifth Asia Symposium on Quality Electronic Design (ASQED 2013), Penang, Malaysia, 26–28 August 2013.
36. Kozuma, M.; Okamoto, Y.; Nakagawa, T.; Aoki, T.; Ikeda, M.; Osada, T.; Kurokawa, Y.; Ikeda, T.; Yamade, N.; Okazaki, Y.; et al. Crystalline In-Ga-Zn-O FET-based configuration memory for multi-context field-programmable gate array realizing fine-grained power gating. *Jpn. J. Appl. Phys.* **2014**, *53*, 04EF12. [CrossRef]
37. Matsuzaki, T.; Onuki, T.; Nagatsuka, S.; Inoue, H.; Ishizu, T.; Ieda, Y.; Yamade, N.; Miyairi, H.; Sakakura, M.; Shionoiri, Y.; et al. A 16-level-cell memory with c-axis-aligned a-b-plane-anchored crystal In-Ga-Zn oxide FET using threshold voltage cancel write method. *Jpn. J. Appl. Phys.* **2016**, *55*, 04EE02. [CrossRef]
38. Kandpal, K. A review of evolution comes in non-volatile semiconductor memories like SONOS with the role of high-k dielectric material. *IOSR J. Eng. IOSRJEN* **2014**, *4*, 13–17. [CrossRef]
39. Lee, M.C.; Wong, H.Y. Threshold voltage instability mechanisms of nitride-based charge trap flash memory—A review. *J. Nanosci. Nanotechnol.* **2014**, *14*, 4799–4812. [CrossRef] [PubMed]
40. Breuil, L.; Lisoni, J.G.; Blomme, P.; Van den Bosch, G.; Van Houdt, J. HfO_2 based high-k inter-gate dielectrics for planar NAND flash memory. *IEEE Electron Device Lett.* **2014**, *35*, 45–47. [CrossRef]
41. Tang, Z.; Liu, Z.; Zhu, X. Progress of high-k dielectric applicable to SONOS-type nonvolatile semiconductor memories. *Trans. Electr. Electron. Mater.* **2010**, *11*, 155–165. [CrossRef]

42. Jeong, S.; Jang, S.; Han, H.; Kim, H.; Choi, C. C-axis aligned crystalline indium-gallium-zinc oxide (CAAC-IGZO) and high-k charge trapping film for flash memory application. *J. Alloys Compd.* **2021**, *888*, 161440. [CrossRef]
43. Linfeng, L.; Peng, J. High-Performance Indium-Gallium-Zinc-Oxide thin-film transistors based on anodic aluminum oxide. *Trans. Electron Device* **2011**, *58*, 1452–1455. [CrossRef]
44. Li, Q.; Yu, Y.-H.; Bhatia, C.S.; Marks, L.D.; Lee, S.C.; Chung, Y.W. Low-temperature magnetron sputter-deposition, hardness, and electrical resistivity of amorphous and crystalline alumina thin films. *J. Vac. Sci. Technol. A Vac. Surf. Films* **2000**, *18*, 2333–2338. [CrossRef]
45. Fulton, C.C.; Lucovsky, G.; Nemanich, R.J. Electronic properties of the Zr-ZrO2-SiO2-Si(100) gate stack structure, J. *Appl. Phys.* **2006**, *99*, 063708. [CrossRef]
46. Lee, C.B.; Kang, B.S.; Benayad, A.; Lee, M.J.; Ahn, S.-E.; Kim, K.H.; Stefanovich, G.; Park, Y.; Yoo, I.K. Effects of metal electrodes on the resistive memory switching property of NiO thin films. *Appl. Phys. Lett.* **2008**, *93*, 042115. [CrossRef]
47. Nomura, K.; Kamiya, T.; Hosono, H. Highly stable amorphous In-Ga-Zn-O thin-film transistors produced by eliminating deep subgap defects. *Appl. Phys. Lett.* **2011**, *99*, 053505. [CrossRef]
48. Zan, H.W.; Yeh, C.-C.; Meng, H.-F.; Tsai, C.-C.; Chen, L.-H. Achieving high field-effect mobility in amorphous indium-gallium-zinc oxide by capping a strong reduction layer. *Adv. Mater.* **2012**, *24*, 3509–3514. [CrossRef]
49. Rajachidambaram, M.S.; Pandey, A.; Vilayurganapathy, S.; Nachimuthu, P.; Thevuthasan, S.; Herman, G.S. Improved stability of amorphous zinc tin oxide thin film transistors using molecular passivation. *Appl. Phys. Lett.* **2013**, *103*, 171602. [CrossRef]
50. Robertson, J.; Guo, Y. Light induced instability mechanism in amorphous InGaZn oxide semiconductors. *Appl. Phys. Lett.* **2014**, *104*, 162102. [CrossRef]
51. Ma, P.; Du, L.; Wang, Y.; Jiang, R.; Xin, Q.; Li, Y.; Song, A. Low voltage operation of IGZO thin film transistors enabled by ultrathin Al2O3 gate dielectric. *Appl. Phys. Lett.* **2018**, *112*, 023501. [CrossRef]
52. Hwang, E.S.; Kim, J.S.; Jeon, S.M.; Lee, S.J.; Jang, Y.; Cho, D.Y.; Hwang, C.S. $In_2Ga_2ZnO_7$ oxide semiconductor-based charge trap device for NA for NAND flash memory. *Nanotechnology* **2018**, *29*, 155203. [CrossRef]
53. Lei, H.; Qin, P.; Ke, W.; Guo, Y.; Dai, X.; Chen, Z.; Wang, H.; Li, B.; Zheng, Q.; Fang, G. Performance enhancement of polymer solar cells with high work function CuS modified ITO as anodes. *Org. Electron* **2015**, *22*, 173–179. [CrossRef]
54. Kumar, B.; Kauzhik, B.K.; Negi, Y.S. Perspectives and challenges for organic thin film transistors: Materials, devices, processes and applications. *J. Mater. Sci. Mater. Electron.* **2014**, *25*, 1–30. [CrossRef]